Quantitative Analysis of Nanorod Aggregation and Morphology from Scanning Electron Micrographs using SEMseg

Rashad Baiyasi,^a Miranda J. Gallagher,^b Lauren A. McCarthy,^b Emily K. Searles,^b Qingfeng Zhang,^{b,c} Stephan Link,^{a,b,c} Christy F. Landes *a,b,c,d

^aDepartment of Electrical and Computer Engineering, Rice University, MS 366, Houston, Texas 77005, United States

^bDepartment of Chemistry, Rice University, MS 60, Houston, Texas 77005, United States
^cSmalley-Curl Institute, Rice University, Houston, Texas 77005, United States
^dDepartment of Chemical and Biomolecular Engineering, Rice University, Houston, Texas 77005, United States

KEYWORDS scanning electron microscopy, nanoparticle aggregation, nanoparticle assembly, image processing, image segmentation.

ABSTRACT

General methods to achieve better physical insight about nanoparticle aggregation and assembly are needed because of the potential role of aggregation in a wide range of materials, environmental, and biological outcomes. Scanning electron microscopy (SEM) is fast and affordable compared to transmission electron microscopy, but SEM micrographs lack contrast and resolution due to lower beam energy, topographic contrast, edge effects, and charging. We present a new segmentation algorithm called SEMseg that is robust to the challenges inherent in SEM micrograph analysis and demonstrate its utility for analyzing gold (Au) nanorod aggregates. SEMseg not only supports nanoparticle size analysis for dispersed nanoparticles, but also discriminates between nanoparticles within an aggregate. We compare our algorithm to those incorporated into the commonly used software ImageJ and demonstrate improved segmentation of aggregate structures. New physical insight about aggregation is demonstrated by the introduction of an order parameter describing side-by-side structure in nanoparticle aggregates. We also present the segmentation and fitting algorithms included in SEMseg within a user-friendly graphical user interface. The resulting code is provided with an open-source interface to provide quantitative image processing tools for researchers to characterize both dispersed nanoparticles and nanoparticle assemblies in SEM micrographs with high throughput.

INTRODUCTION

⁴¹ and electron microscopy. ⁴² The quantitative parameters provided by these methods (e.g., radius of gyration, radial distribution, fractal dimension) ⁴³⁻⁴⁷ provide averaged descriptions of the long-range structure and can under- or over- reflect underlying heterogeneity, small aggregates and assemblies, or short-range order.

Scanning electron microscopy (SEM) is a fast and affordable means of imaging nanoparticle assemblies. Electron micrographs are regularly used to measure nanoparticle size/morphology, 8, 33, 37, 48-50 surface coverage, 51 and the effectiveness of nanoparticle assembly methods. 52 More expensive and time consuming, transmission electron microscopy (TEM) produces high-contrast and high-resolution micrographs suitable for quantitative structural analysis, whereas SEM has lower contrast and resolution and exhibits topographic contrast, edge effects, and charging. 53 The low relative quality of SEM generally relegates it to qualitative sample assessment, but image segmentation algorithms 48, 54-61 offer the possibility of quantitative SEM analysis that may not be provided by common tools included in programs such as ImageJ or Photoshop. 62

Image segmentation is an image processing method⁶³⁻⁶⁴ that classifies each pixel in an image as belonging to one of some number of object classes.⁶⁵ The positions and intensities of pixels assigned to an object via segmentation provide quantitative descriptors that can be extracted from segmented images with high throughput. Segmentation algorithms are problem-specific, utilizing various image processing techniques depending on the complexity of the segmentation problem.^{48,54-61} Compared to well-separated nanoparticles, segmentation of aggregated nanoparticles is a greater challenge because algorithms can over- or under-segment closely spaced nanoparticles.⁶⁶ The challenges involved in categorizing long- and short-range ordering,^{38,67} relative orientations,^{21,68-71} surface-chemistry driven forces,^{40,69} and optical properties^{7,70,72} motivate the

need for image-processing algorithms that can accurately segment nanoparticles in aggregates and assemblies.

Here we present SEMseg, a segmentation algorithm that is robust to the challenges inherent in analyzing SEM micrographs of nanoparticle aggregates to demonstrate principles of effective segmentation algorithm design and to provide a practical tool for nanoparticle aggregate characterization. The presented algorithm consists of three steps: background masking, the marker-controlled watershed method, and nanorod fitting. SEMseg is designed to be robust for a variety of nanoparticle shapes, preparations, and aggregation scales, and also offers user optimization through a graphical user interface (GUI) called SEMseg. We combine SEMseg with a fitting function appropriate for rod- or circle-shaped nanoparticle profiles, but the algorithm can be generalized to other nanoparticle geometries by changing the fitting function. The nanoparticle fits are used to characterize detected nanoparticles, and calculation of a side-by-side order parameter is introduced as a possible means of characterizing intra-aggregate structure.

EXPERIMENTAL METHODS

Nanoparticle Aggregate Preparation. Nanorod aggregate samples were prepared based on our previously published protocol⁷ by a 1:1 mixture of ~1 nM mercaptoundecyltrimethylammonium bromide (MUTAB) functionalized Au nanorods (NRs, C12-40-750, Nanopartz Inc.) with 1.5 μ M BSA (lyophilized powder, \geq 96%, Sigma-Aldrich, Inc.) in phosphate buffer (0.1M, pH 7.5, Sigma-Aldrich, Inc.). 10 μ L of commercial MUTAB-Au NRs solution were mixed with 90 μ L 0.1 mM hexadecyltrimethylammonium bromide (CTAB, \geq 99%, Sigma Aldrich) before use for aggregation. Nanorods were given 2, 5, or 7 minutes of aggregation time. Au nanorod aggregates were spincast (500 rpm for 15 s followed by 2500 rpm for 60 s) onto oxygen plasma cleaned (2 min) ITO

coated microscope slides (CG-50IN-S107, $R_s = 8-12 \Omega$, Delta Technologies, Ltd.). Surfactants were not removed from the nanorods prior to imaging.

Dewetted Film Preparation. Nano-island samples characterized with SEMseg were fabricated via dewetting of thin films.⁷³ Electron beam evaporation was used to deposit a 3 nm Au film onto ITO coated glass coverslips (22 × 22 mm) (55 Ω /sq., Evaporated Coatings Inc.). The Au films were annealed on a hot plate for 12 h at 150°C. Spherical Au nano-islands, supporting a surface plasmon resonance, were formed on the surface of the ITO substrate.

Electron-Beam Lithography. Au nanorod dimers with approximately 40 nm widths, 80 nm lengths, and 20 nm gaps were fabricated in a method similar to that previously described. Heighly, ITO coated microscope slides (CG-50IN-S107, R_s = 8-12 Ω, Delta Technologies, Ltd.) were cleaned through 10 min sonication steps in 2% Liquinox® detergent, Milli-Q® water, and ethanol (Decon Labs, Inc., 190 proof). Next, positive-tone electron resist (polymethyl methacrylate A4, Kayaku Advanced Materials, Inc.) was spin-coated at 3000 rpm for 60 s followed by baking at 180°C for 90 s. Patterns were written via a Nanometer Pattern Generation System on an FEI QuantaTM 650 SEM with a voltage of 30 kV, a beam current of 40 pA, and a working distance of 7 mm. The beam-exposed resist was then developed in a 1:3 methyl isobutyl ketone: isopropanol solution for 70 s followed by a 60 s rinse in isopropanol. Finally, an electron beam evaporator was used to deposit a 40 nm Au film. Lift-off was completed by an overnight soak in acetone followed by gentle sonication and drying with a stream of N₂. The structures were then imaged on the same microscope used for fabrication under the same conditions.

Electron Microscopy. SEM micrographs of Au nanorod aggregates for 2-, 5-, and 7-min aggregation time, lithographic rods, and nanoislands were collected with a FEI Helios Nanolab 660 Dualbeam SEM (10 kV, Thermo Fisher Scientific).

COMPUTATIONAL METHODS

ImageJ Segmentation and Fitting. ImageJ analysis consisted of two applications of the builtin *Smooth* process, a manually selected *Threshold* adjustment, the binary *Watershed* process, and running the *Analyze Particles* routine.

SEMseg: an Algorithm for Segmentation and Fitting of Nanoparticle Aggregates

SEM micrographs were processed using SEMseg, a custom-designed GUI for image processing and analysis in MATLAB. The methods in this section describe the key steps of the segmentation and fitting algorithms included in SEMseg. See Supporting Information for further detail and instructions on the GUI SEMseg and its operation. SEMseg is available for download through a GitHub repository (https://github.com/LandesLab?tab=repositories).

Weak contrast of inter-particle boundaries and topographical contrast variation on nanoparticle surfaces in SEM micrographs of aggregates and assemblies is the first challenge for segmentation. SEM micrographs occur on nanorod ends and edges and do not directly correspond to topographic features (Figure 1a). These bright edges can result in interparticle boundaries with higher intensities than regions inside of particles, inhibiting traditional intensity thresholding techniques from isolating single nanoparticles (Figure S1). High-frequency variation in topographical contrast leads to erroneous edge detection and contributes to oversegmentation, in which single nanoparticles are subdivided into multiple objects. These challenges are overcome in SEMseg through a combination of background masking, internal and external

marker calculation, the watershed transform of the gradient magnitude, and nanorod fitting and parameter estimation, as presented in the workflow outlined in Figure 1.

Background Masking

Background masking (Figure 1b) removes background features and isolates nanoparticles, a step that is crucial for SEM samples, which require conductive substrates such as indium tin oxide (ITO) coated glass that has distinct grain edges (Figure S1a). First, raw micrographs are cropped to isolate the aggregate of interest, converted to grayscale, and scaled so intensities fall in the range [0, 1]. The spatial scale of each micrograph is maintained so the pixel-to-nanometer conversion provided by the SEM scale bar is still applicable. ITO grain structure is suppressed through the morphological opening operation⁵⁸ (Figure S2) performed on the grayscale micrograph. The radius of the circular morphological structuring element, the intensity threshold, and the minimum size threshold are variable parameters of the background masking operation. The radius of the structuring element can be set manually or can be estimated by a parameter sweep as shown in Figure S3. The threshold value of 0.2 used for this study was found to be robust for a variety of micrograph contrasts. The background mask is used with the preprocessed micrograph to isolate nanoparticle aggregates for the calculation of internal and external markers described below.

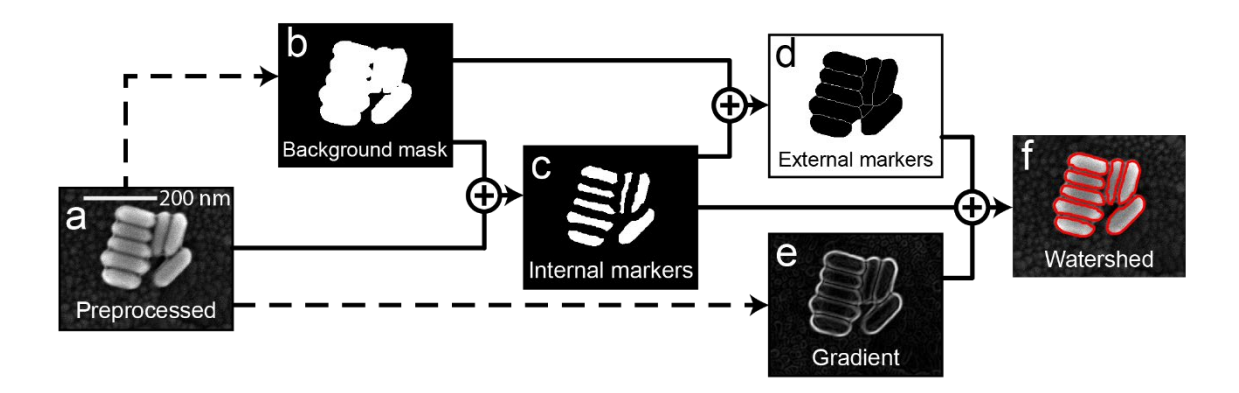


Figure 1. SEMseg segmentation algorithm for SEM micrographs of planar nanorod aggregates. Dashed lines represent image processing applied to a single micrograph and plus symbols indicate multiple sub-micrographs combined together before image processing. (a) Preprocessing includes cropping the SEM micrograph and scaling intensity values to [0,1]. (b) Background masking isolates nanoparticles from the ITO substrate. (c) Internal markers for each nanoparticle are calculated by sharpening and cleaning the preprocessed micrograph (a) masked with (b). (d) External markers indicating the inter-nanoparticle boundaries and background. (e) Gradient image calculated from the preprocessed micrograph (a) using the Sobel method. (f) Watershed segmentation contours (red outlines) overlaid on the preprocessed micrograph.

Internal and External Marker Calculation

Artificially imposed minima that mark the interior of each nanoparticle and the boundaries between them, called internal and external markers, respectively, are established to identify each individual nanoparticle in an aggregate or assembly. The first step in internal marker calculation (Figure 1c) is to increase the contrast between nanoparticle surfaces and boundaries by unsharp masking using the MATLAB imsharpen function. Unsharp masking enhances contrast by summing an image and the output of a high-pass filter. The radius of the unsharp mask determines the scale on which the mask increases contrast and should be close to the mean separation between nanoparticles in the micrographs (~8 pixels here). The strength of the unsharp masking is determined by the intensity parameter, and a value on the order of ~70 was found to provide sufficient contrast for thresholding to separate individual nanoparticle markers. We clean up the noisy sharpened image (Figure S4) and obtain the final internal markers shown in Figure 1c using

morphological operators. We calculate external markers using the union of the internal markers and the complement of the background mask, reduced to a morphological skeleton with a single-pixel width using the bwskel function in MATLAB.⁵⁸ The resultant morphological skeleton is combined with the complement of the background mask to prevent the segmentation of the background, resulting in the external markers shown in Figure 1d.

Watershed Transform of the Gradient Magnitude

We implement a variation of the watershed transform for segmentation using internal and external markers, ^{56,76} functioning effectively as the flooding of a topographic landscape. ⁵⁷ For this application, we define the height of this topographic landscape as the gradient magnitude of the SEM micrograph, shown in Figure 1e. The minima in the gradient image, called catchment basins, are treated as the bottoms of water pools that are filled up by the watershed transform. Wherever the water from two pools touch, a crest line is drawn to define segmentation contours between them. Ideally, each object in a micrograph would have a single local minimum near its center and local minima around the edges. The noise and intensity variation in SEM micrographs result in over-segmentation (Figure S5), but this problem is overcome by performing the watershed after the internal and external markers⁵⁷ are calculated (Figure 1c–d). The internal and external markers are combined through union and imposed as minima on the gradient magnitude image using the imimposemin function in the MATLAB Image Processing Toolbox. Imposing minima defines the catchment basin for each nanoparticle using the calculated markers. The watershed transform is applied to this augmented gradient image and the contours of each contiguous region of pixels provides the nanoparticle segmentation contours as shown in Figure 1f. Nanorod contours are fit to a stadium geometry to estimate parameters describing each nanorod in the aggregate, as discussed below.

Nanorod Fitting

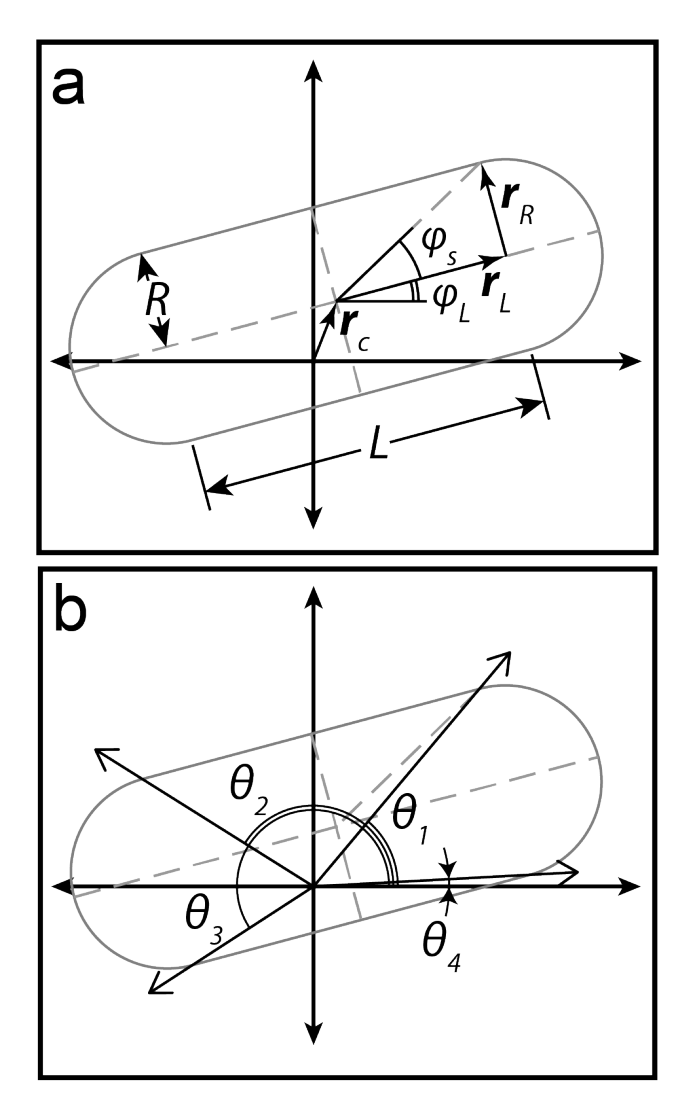


Figure 2. Calculating nanorod dimensions and orientation using a stadium model that is fit in polar coordinates. (a) Vectors defining the stadium fit: offset between estimated centroid and actual centroid, $\mathbf{r}_c = \langle x_0, y_0 \rangle$, nanorod length and orientation vector, \mathbf{r}_L , and nanorod endcap vector, \mathbf{r}_R . The nanorod length is L+2R and the width is 2R, where $L=2 \cdot |\mathbf{r}_L|$ and $R=|\mathbf{r}_R|$. (b) Angles describing the limits of the piecewise function defining the stadium model: $\theta_1=\Phi\{\vec{r}_c+\vec{r}_L+\vec{r}_R\}$, $\theta_2=\Phi\{\vec{r}_c-\vec{r}_L+\vec{r}_R\}$,

 $\theta_3 = \Phi\{\vec{r}_c - \vec{r}_L - \vec{r}_R\}, \ \theta_4 = \Phi\{\vec{r}_c + \vec{r}_L - \vec{r}_R\}, \ \text{where} \ \Phi\{\vec{z}\} = \arctan\left(\frac{z_y}{z_x}\right).$ We define the piecewise function of the stadium model in the Supporting Information.

Accurate fitting requires a functional model that appropriately describes the nanoparticle morphology, 48 which, in the case of nanorods imaged by SEM, is best described as the twodimensional projection of a hemispherically-capped cylinder, 77 called a stadium (Figure 2). Because a functional definition of a stadium is, to the best of our knowledge, not defined in the literature, we derived our own expression. The stadium is a piecewise function defined by five parameters, $(x_0, y_0, \varphi, L, R)$, which describe the x and y coordinates of the nanorod center x_0, y_0 , the orientation φ of the nanorod axis, the length L of the body (neglecting the end-caps), and the radius R of the end-caps, respectively. Figure 2 shows the polar formulation of the stadium for fitting nanoparticle contours using vector notation. We express the segmentation contour in polar coordinates as $\rho(\theta)$ by calculating the distance, ρ , and the angle, θ , relative to the nanoparticle's centroid for each pixel on the contour. 48 The origin of the coordinate system is the centroid of the watershed contour points, with (x_0, y_0) accounting for the deviation from the true nanoparticle centroid and φ representing the rotation about the true nanoparticle centroid. Figure 2b illustrates the angles that define the intervals of the piecewise function, measured relative to the estimated centroid from the watershed contours. The segmentation contour for each nanorod is iteratively fit to the stadium model using nonlinear least squares fitting in MATLAB. We adopt the least absolute residual method to make the fit robust to outliers that may be present on the nanorod contour. The stadium function is also appropriate for fitting nanoparticles with circular profiles, as a stadium where L = 0 is simply a circle.

RESULTS AND DISCUSSION

Nanoparticle Parameter Estimation

With the segmentation and fitting performed by SEMseg, structural parameters of nanoparticles (e.g., centroid position, major and minor axis, orientation) can be calculated from the stadium parameters as described in Figure 2 and in the Supporting Information. Micrographs segmented using ImageJ and SEMseg are shown in Figure S6 and Figure 3, respectively. Table 1 gives the mean and standard deviation of the nanoparticle parameters calculated with each method. The inset of Figure 3a compares estimated lengths using SEMseg and manually measured lengths in ImageJ for 58 nanorods, demonstrating accurate nanorod parameter estimation with a root-mean-square error of 3.2 nm.

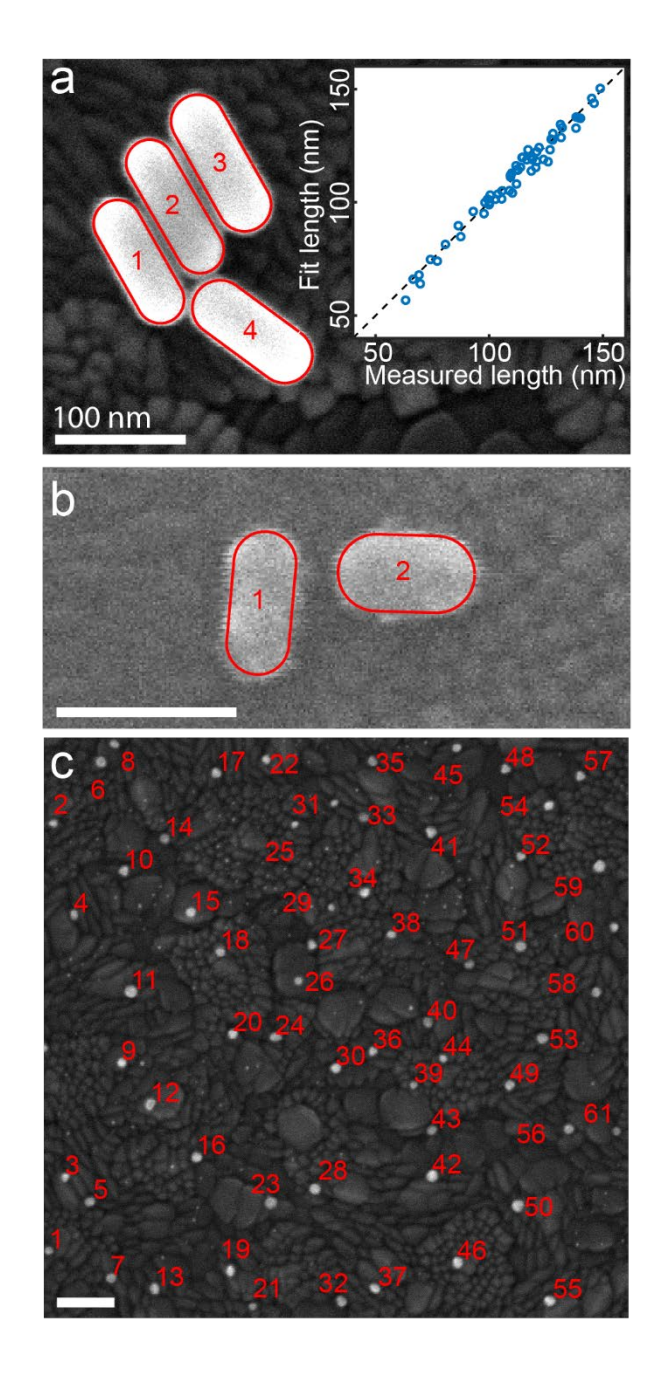


Figure 3. Output from SEMseg analysis of example nanoparticle images. (a) Colloidal Au nanorod aggregate, (b) lithographic Au nanorod dimer, and (c) Au nanoislands formed through dewetting of a 3 nm Au film on an ITO substrate. All scale bars are 100 nm. Red outlines depict the stadium fit for each nanoparticle. Outlines are omitted from (c) to improve particle visibility. Individual nanoparticles were segmented using

SEMseg, a GUI implementation of the segmentation and stadium fitting algorithm. Tabulated data shown in Table 1 are calculated from the nanoparticle fits, summarizing particle parameters that can be used for further analysis. Inset of (a) shows SEMseg fit nanorod length vs. nanorod lengths manually measured in ImageJ for N=58 nanorods, showing the accuracy of SEMseg (root-mean-square error = 3.2 nm for \sim 111 nm long nanorods).

Table 1. Sample output of nanoparticle parameters estimated from segmentation and fitting performed on SEM micrographs[†]

Sample	# particles	Major Axis	Minor Axis	Area	Median gap
ImageJ segmentation					
A	6	$82 \pm 28 \text{ nm}$	$48 \pm 3 \text{ nm}$	$(3 \pm 1) \times 10^3 \text{ nm}^2$	n/a
В	2	$87 \pm 5 \text{ nm}$	$48\pm 6 \ nm$	$(3.3 \pm 0.2) \times 10^3 \text{ nm}^2$	n/a
C	69	$15 \pm 5 \text{ nm}$	$14\pm4\;nm$	$(1.8 \pm 0.9) \times 10^2 \text{ nm}^2$	n/a
SEMseg					
A	4	$109 \pm 6 \text{ nm}$	$39 \pm 3 \text{ nm}$	$(3.9 \pm 0.4) \times 10^3 \text{ nm}^2$	8 nm
В	2	$79\pm 3\ nm$	$39 \pm 6 \ nm$	$(2.7 \pm 0.2) \times 10^3 \text{ nm}^2$	24 nm
C	61	$14\pm2\;nm$	$11 \pm 2 \text{ nm}$	$(1.3 \pm 0.4) \times 10^2 \text{ nm}^2$	87 nm

[†] Nanoparticle parameter estimates calculated using ImageJ and SEMseg. Parameters are listed as mean value and standard deviation where appropriate. Samples (A–C) refer to Figure 3a–c, respectively.

Calculating nanoparticle parameters from electron micrographs in an automated manner enables high throughput analysis of different types of nanoparticle assemblies without compromising accuracy. SEMseg can be applied to densely packed nanoparticles (Figure 3a), and also for samples with dispersed nanoparticles (Figure 3b–c). Due to the general nature of the watershed

transform, this algorithm could also be applicable to images of particles with edges defined by an intensity gradient, such as those collected by atomic force microscopy, opening up the possibilities of improving analysis of other broader types of imaging platforms.

SEMseg effectively analyzes aggregated nanoparticles in micrographs that cannot be segmented by other widely available tools (Figure 4). For example, the open-source software ImageJ is effective for segmenting well-dispersed particles but generally fails to segment individual nanoparticles in aggregates or assemblies that SEMseg can accurately segment (Figure 4a, Figure S6). The watershed implementation built into ImageJ, based on the distance transform, leads to over-segmentation of oblong particles (Figure 4b, Figure S6a), while thresholding without the watershed transform leads to under-segmentation of aggregated particles. Similar to the stadium fitting implemented in SEMseg, the Analyze Particles ImageJ routine fits each contiguous patch of pixels to an ellipse (Figure 4d) and calculates properties such as the short and long axes and orientation, as summarized in Table 1. Other tools in ImageJ can be used to aid in segmenting particles, such as morphological operators and filtering to clean images, or manual input to segment or throw out particles. 42, 65 Machine learning segmentation methods relying on handlabeled training data have also been implemented in ImageJ.⁶¹ Other published algorithms that segment closely spaced nanoparticles require the high resolution and contrast of TEM micrographs 48,78 and do not function for SEM micrographs. SEMseg is a training-free alternative that can successfully segment both dispersed nanoparticles and nanoparticle aggregates from SEM micrographs.

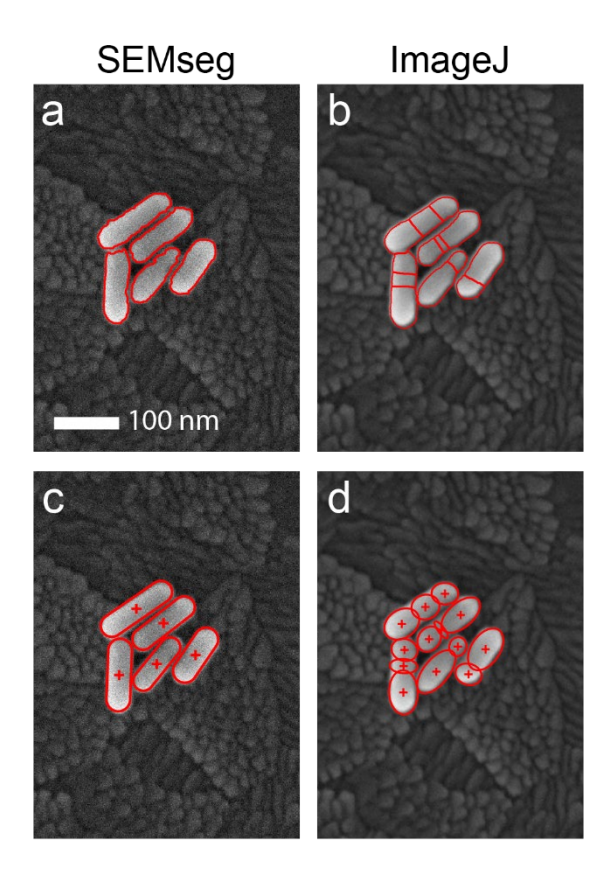


Figure 4. Comparison of SEMseg and ImageJ for nanorod aggregate watershed segmentation by displaying the resultant mask over the preprocessed image. (a-b) Watershed segmentation contours using SEMseg (a) and built-in ImageJ methods (b). (c) Segmentation contours in (a) fit to the stadium model included in SEMseg. (d) Segmentation contours in (b) fit to an elliptical model using the ImageJ Analyze Particles routine. Red crosses in (c-d) indicate the calculated centroid of each segmented region. As shown in (b) and (d), the watershed algorithm implemented in ImageJ leads to over-segmentation.

Describing Ordering in Nanorod Aggregates

By allowing accurate segmentation in SEM micrographs, SEMseg can provide insight into previously unknown structural order of small aggregates of nanorods (Figure 5). The two-

dimensional nematic liquid crystal order parameter, $S_{2D} = \langle \cos 2\theta \rangle$ suitably describes order in nanorod chains and large nanorod assemblies with long-range order, where an S_{2D} of 0 is fully disordered and S_{2D} of 1 is ordered. The ordering described by S_{2D} is a measure of uniformity of orientation, where the orientation of each nanoparticle long axis is compared to the average orientation vector of all nanoparticles, called the nematic director. S_{2D}^{52} is not a suitable descriptor for small aggregates and assemblies with differently-oriented domains. We demonstrate the ability to identify new types of ordering within aggregate in Figure 5a-b, where aggregates both with and without side-by-side ordering lead to the same S_{2D} order parameter values. We quantify the ordering in various unaligned domains defining a side-by-side order parameter S_R given in Equation 1,7

$$S_R = \frac{\sum_{i=1}^{N_{nr}} M_i}{2(N_{nr}-1)},$$
 Equation 1

where N_{nr} is the number of nanorods in the aggregate and M_i is the number of side-by-side nearest neighbors for nanorod $i \in \{1,2,...,N_{nr}\}$. We define side-by-side nanorods as nearest neighbors that have an orientation within 10° of each other and where the vector connecting their midpoints, projected onto the long nanorod orientation, is less than half the longer nanorod's length. $S_R = 1$ for the most ordered structure, is a continuous line of side-by-side nanorods, while a disordered aggregate with no side-by-side ordering has $S_R = 0$.

By using S_R as an order parameter, we find Au nanorod aggregates that appear disordered by S_{2D} may contain side-by-side ordering structure (Figure 5c). We have previously applied S_R in the reported use of biomolecules as templates for chiral nanoparticle assembly⁷ to measure side-by-side arrangement of nanorods. To demonstrate the effectiveness of SEMseg for quantifying side-by-side ordering in experimental nanorod aggregates, Figure 5d–e compares S_{2D} and S_R for a population of bovine serum albumin (BSA)-induced nanorod aggregates. While S_{2D} produces a

broad distribution of order parameters across the population of aggregates, S_R displays a comparatively narrow range of ordering. This narrower distribution is a boon for statistical analysis of aggregate population ordering, and is likely due to the sensitivity of S_R to side-by-side ordering even when split up over multiple, differently oriented domains. By utilizing SEMseg and establishing quantitative image analysis parameters, it may be possible to attain insight into previously unknown aggregate and assembly structures from SEM micrographs.

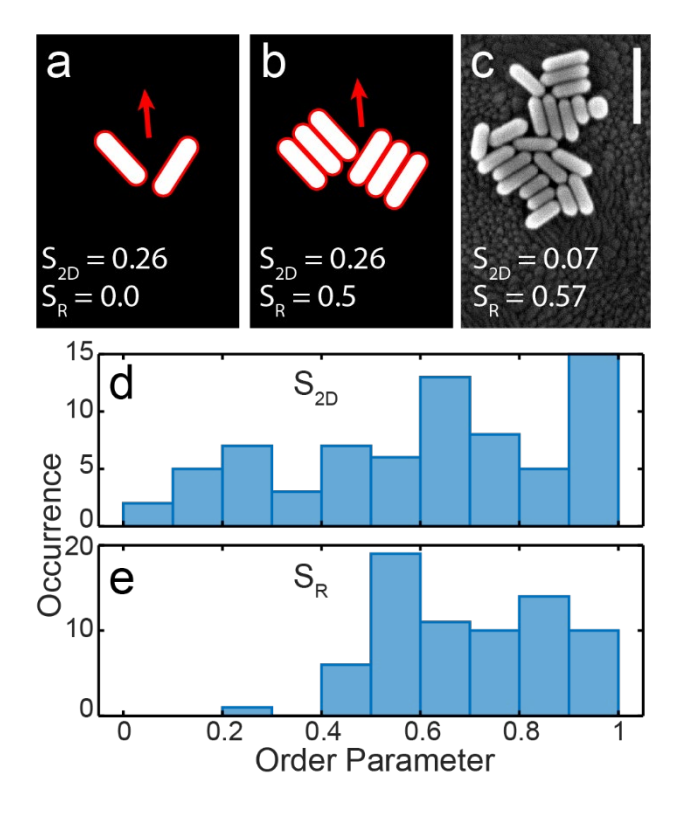


Figure 5. Comparison of the order parameters S_R and S_{2D} to describe side-by-side ordering in segmented nanorod aggregate images. (a–b) Simulated nanorod aggregates where S_R quantifies the side-by-side ordering that is not described by S_{2D}. Red outlines show nanorod fit results using SEMseg and red arrows indicate the average nanorod orientation. (c) SEM micrograph of an Au nanorod aggregate with S_{2D} and S_R values that lead to different interpretations of the aggregate's ordering (scale bar 200 nm). S_{2D} reports an almost completely disordered aggregate, while S_R reveals the

prevalence of side-by-side arrangement in the aggregate structure. (d–e) Histograms of S_{2D} and S_R values, respectively, for a population of Au nanorods aggregates (N=71) formed by the addition of BSA (See Experimental Methods).

CONCLUSION

Nanoparticle aggregation and assembly is an area of active research that benefits from the availability of analysis tools and software that provide insight into their structure. We described an image segmentation algorithm with a GUI implementation for SEM micrographs, called SEMseg. SEMseg can segment well-dispersed nanoparticles and lithographic structures similarly to the popular software ImageJ, with the additional capability of distinguishing individual nanorods in closely packed assemblies and aggregates to quickly determine the size and orientation of each particle and the gap-size between particles. We derived a nanorod fit model using the stadium geometry for parameterizing nanorods and discussed the effectiveness of the side-by-side order parameter S_R for providing structural insight into populations of nanoparticle aggregates. Our open-source GUI for SEMseg provides a resource for researchers to explore nanoparticle aggregation and perform nanoparticle size analysis using cost-effective SEM with high throughput compared to other methods. Dissemination of such high throughput computational methods opens the door for statistical analysis of aggregate structure without the prohibitive time expense of manual segmentation of large datasets.

Conflicts of interest

There are no conflicts of interest to declare.

ACKNOWLEDGEMENT

This material is based upon work supported by, or in part by, the U. S. Army Research

Laboratory and the U. S. Army Research Office under grant number ARO W911NF1910363.

Funding for this work provided by the National Science Foundation to S.L. (CHE1727122), the

Robert A. Welch Foundation to C.L. (C-1664) and to S.L. (C-1781). L.A.M. gratefully

acknowledges support from the National Science Foundation Graduate Research Fellowship

Program (1842494). This work was conducted in part using resources of the Shared Equipment

Authority at Rice University.

AUTHOR INFORMATION

Corresponding Author

* Corresponding author E-mail: cflandes@rice.edu

Author Contributions

The manuscript was written through contributions of all authors. All authors have given approval

to the final version of the manuscript.

ASSOCIATED CONTENT

Supporting Information

The Supporting Information is available free of charge at https://pubs.acs.org/doi/

Stadium fit model formulation; figures showing intensity thresholding in SEM micrographs,

morphological operators, parameter sweep for structure element determination, unsharp masking,

20

over-segmentation with watershed transformation, example segmentation in ImageJ; end-user instructions for SEMseg nanoparticle segmentation GUI.

REFERENCES

- 1. Murray, C. B.; Kagan, C. R.; Bawendi, M. G. Synthesis and Characterization of Monodisperse Nanocrystals and Close-Packed Nanocrystal Assemblies. *Annu. Rev. Mater. Sci.* **2000**, *30*, 545-610.
- 2. Jones, M. R.; Osberg, K. D.; Macfarlane, R. J.; Langille, M. R.; Mirkin, C. A. Templated Techniques for the Synthesis and Assembly of

Plasmonic Nanostructures. Chem. Rev. 2011, 111, 3736-3827.

- 3. Stolarczyk, J. K.; Deak, A.; Brougham, D. F. Nanoparticle Clusters: Assembly and Control Over Internal Order, Current Capabilities, and Future Potential. *Adv. Mater.* **2016**, *28*, 5400-5424.
- 4. Grzelczak, M.; Perez-Juste, J.; Mulvaney, P.; Liz-Marzan, L. M. Shape Control in Gold Nanoparticle Synthesis. *Chem. Soc. Rev.* **2008,** *37*, 1783-1791.
- 5. Thirumalairajan, S.; Girija, K.; Ganesh, I.; Mangalaraj, D.; Viswanathan, C.; Balamurugan, A.; Ponpandian, N. Controlled Synthesis of Perovskite LaFeO3 Microsphere Composed of Nanoparticles via Self-Assembly Process and Their Associated Photocatalytic Activity. *Chem. Eng. J.* **2012**, *209*, 420-428.
- 6. Osterloh, F. E. Solution Self-Assembly of Magnetic Light Modulators From Exfoliated Perovskite and Magnetite Nanoparticles. *J. Am. Chem. Soc.* **2002**, *124*, 6248-6249.
- 7. Zhang, Q.; Hernandez, T.; Smith, K. W.; Hosseini Jebeli, S. A.; Dai, A. X.; Warning, L.; Baiyasi, R.; McCarthy, L. A.; Guo, H.; Chen, D. H., et al. Unraveling the Origin of Chirality from Plasmonic Nanoparticle-Protein Complexes. *Science* **2019**, *365*, 1475-1478.
- 8. Hu, M.; Novo, C.; Funston, A.; Wang, H. N.; Staleva, H.; Zou, S. L.; Mulvaney, P.; Xia, Y. N.; Hartland, G. V. Dark-Field Microscopy Studies of Single Metal Nanoparticles: Understanding the Factors That Influence the Linewidth of the Localized Surface Plasmon Resonance. *J. Mater. Chem.* **2008**, *18*, 1949-1960.
- 9. Chang, W. S.; Slaughter, L. S.; Khanal, B. P.; Manna, P.; Zubarev, E. R.; Link, S. One-Dimensional Coupling of Gold Nanoparticle Plasmons in Self-Assembled Ring Superstructures. *Nano Lett.* **2009**, *9*, 1152-1157.
- 10. Hamon, C.; Novikov, S. M.; Scarabelli, L.; Solis, D. M.; Altantzis, T.; Bals, S.; Taboada, J. M.; Obelleiro, F.; Liz-Marzan, L. M. Collective Plasmonic Properties in Few-Layer Gold Nanorod Supercrystals. *ACS Photonics* **2015**, *2*, 1482-1488.
- 11. Jiang, J. K.; Oberdorster, G.; Biswas, P. Characterization of Size, Surface Charge, and Agglomeration State of Nanoparticle Dispersions for Toxicological Studies. *J. Nanopart. Res.* **2009**, *11*, 77-89.
- 12. Tsugita, M.; Morimoto, N.; Nakayama, M. SiO2 and TiO2 Nanoparticles Synergistically Trigger Macrophage Inflammatory Responses. *Part. Fibre Toxicol.* **2017**, *14*, 11.
- 13. Albanese, A.; Chan, W. C. Effect of Gold Nanoparticle Aggregation on Cell Uptake and Toxicity. *ACS Nano* **2011**, *5*, 5478-5489.
- 14. O'Melia, C. R. Particle—Particle Interactions in Aquatic Systems. *Colloids Surf.* **1989,** *39*, 255-271.

- 15. Grzelczak, M.; Vermant, J.; Furst, E. M.; Liz-Marzan, L. M. Directed Self-Assembly of Nanoparticles. *ACS Nano* **2010**, *4*, 3591-3605.
- 16. Claridge, S. A.; Castleman, A. W., Jr.; Khanna, S. N.; Murray, C. B.; Sen, A.; Weiss, P. S. Cluster-Assembled Materials. *ACS Nano* **2009**, *3*, 244-255.
- 17. Hamon, C.; Postic, M.; Mazari, E.; Bizien, T.; Dupuis, C.; Even-Hernandez, P.; Jimenez, A.; Courbin, L.; Gosse, C.; Artzner, F., et al. Three-Dimensional Self-Assembling of Gold Nanorods with Controlled Macroscopic Shape and Local Smectic B Order. *ACS Nano* **2012**, *6*, 4137-4146.
- 18. Xie, Y.; Guo, S.; Guo, C.; He, M.; Chen, D.; Ji, Y.; Chen, Z.; Wu, X.; Liu, Q.; Xie, S. Controllable Two-Stage Droplet Evaporation Method and its Nanoparticle Self-Assembly Mechanism. *Langmuir* **2013**, *29*, 6232-6241.
- 19. Taheri, S. M.; Michaelis, M.; Friedrich, T.; Forster, B.; Drechsler, M.; Romer, F. M.; Bosecke, P.; Narayanan, T.; Weber, B.; Rehberg, I., et al. Self-Dssembly of Smallest Magnetic Particles. *Proc. Natl. Acad. Sci. U. S. A.* **2015**, *112*, 14484-14489.
- 20. Baker, J. L.; Widmer-Cooper, A.; Toney, M. F.; Geissler, P. L.; Alivisatos, A. P. Device-Scale Perpendicular Alignment of Colloidal Nanorods. *Nano Lett.* **2010**, *10*, 195-201.
- 21. Singh, A.; Gunning, R. D.; Sanyal, A.; Ryan, K. M. Directing Semiconductor Nanorod Assembly into 1D or 2D Supercrystals by Altering the Surface Charge. *Chem. Commun.* **2010**, *46*, 7193-7195.
- 22. Singh, A.; Gunning, R. D.; Ahmed, S.; Barrett, C. A.; English, N. J.; Garate, J. A.; Ryan, K. M. Controlled Semiconductor Nanorod Assembly From Solution: Influence of Concentration, Charge and Solvent Nature. *J. Mater. Chem.* **2012**, *22*, 1562-1569.
- 23. Macfarlane, R. J.; Lee, B.; Jones, M. R.; Harris, N.; Schatz, G. C.; Mirkin, C. A. Nanoparticle Superlattice Engineering with DNA. *Science* **2011**, *334*, 204-208.
- 24. Bigioni, T. P.; Lin, X. M.; Nguyen, T. T.; Corwin, E. I.; Witten, T. A.; Jaeger, H. M. Kinetically Driven Self Assembly of Highly Ordered Nanoparticle Monolayers. *Nat. Mater.* **2006**, *5*, 265-270.
- 25. Alvarez-Puebla, R. A.; Agarwal, A.; Manna, P.; Khanal, B. P.; Aldeanueva-Potel, P.; Carbo-Argibay, E.; Pazos-Perez, N.; Vigderman, L.; Zubarev, E. R.; Kotov, N. A., et al. Gold Nanorods 3D-Supercrystals as Surface Enhanced Raman Scattering Spectroscopy Substrates for the Rapid Detection of Scrambled Prions. *Proc. Natl. Acad. Sci. U. S. A.* **2011**, *108*, 8157-8161.
- 26. Bodelon, G.; Montes-Garcia, V.; Lopez-Puente, V.; Hill, E. H.; Hamon, C.; Sanz-Ortiz, M. N.; Rodal-Cedeira, S.; Costas, C.; Celiksoy, S.; Perez-Juste, I., et al. Detection and Imaging of Quorum Sensing in Pseudomonas Aeruginosa Biofilm Communities by Surface-Enhanced Resonance Raman Scattering. *Nat. Mater.* **2016**, *15*, 1203-1211.
- 27. Liu, K.; Zhao, N.; Kumacheva, E. Self-Assembly of Inorganic Nanorods. *Chem. Soc. Rev.* **2011,** *40*, 656-671.
- 28. Rivest, J. B.; Swisher, S. L.; Fong, L. K.; Zheng, H.; Alivisatos, A. P. Assembled Monolayer Nanorod Heterojunctions. *ACS Nano* **2011**, *5*, 3811-3816.
- 29. Auyeung, E.; Morris, W.; Mondloch, J. E.; Hupp, J. T.; Farha, O. K.; Mirkin, C. A. Controlling Structure and Porosity in Catalytic Nanoparticle Superlattices with DNA. *J. Am. Chem. Soc.* **2015**, *137*, 1658-1662.
- 30. Yu, Y.; Ng, C.; Konig, T. A. F.; Fery, A. Tackling the Scalability Challenge in Plasmonics by Wrinkle-Assisted Colloidal Self-Assembly. *Langmuir* **2019**, *35*, 8629-8645.

- 31. Wang, C.; Sang, X.; Gamler, J. T. L.; Chen, D. P.; Unocic, R. R.; Skrabalak, S. E. Facet-Dependent Deposition of Highly Strained Alloyed Shells on Intermetallic Nanoparticles for Enhanced Electrocatalysis. *Nano Lett.* **2017**, *17*, 5526-5532.
- 32. Kirchner, S. R.; Smith, K. W.; Hoener, B. S.; Collins, S. S. E.; Wang, W. X.; Cai, Y. Y.; Kinnear, C.; Zhang, H. Y.; Chang, W. S.; Mulvaney, P., et al. Snapshot Hyperspectral Imaging (SHI) for Revealing Irreversible and Heterogeneous Plasmonic Processes. *J. Phys. Chem. C* **2018**, *122*, 6865-6875.
- 33. Al-Zubeidi, A.; Hoener, B. S.; Collins, S. S. E.; Wang, W.; Kirchner, S. R.; Hosseini Jebeli, S. A.; Joplin, A.; Chang, W. S.; Link, S.; Landes, C. F. Hot Holes Assist Plasmonic Nanoelectrode Dissolution. *Nano Lett.* **2019**, *19*, 1301-1306.
- 34. Hoener, B. S.; Byers, C. P.; Heiderscheit, T. S.; De Silva Indrasekara, A. S.; Hoggard, A.; Chang, W.-S.; Link, S.; Landes, C. F. Spectroelectrochemistry of Halide Anion Adsorption and Dissolution of Single Gold Nanorods. *J. Phys. Chem. C* **2016**, *120*, 20604-20612.
- 35. Korram, J.; Dewangan, L.; Nagwanshi, R.; Karbhal, I.; Ghosh, K. K.; Satnami, M. L. A Carbon Quantum Dot–Gold Nanoparticle System as a Probe for the Inhibition and Reactivation of Acetylcholinesterase: Detection of Pesticides. *New J. Chem.* **2019**, *43*, 6874-6882.
- 36. Lv, J.; He, B. N.; Wang, N.; Li, M.; Lin, Y. L. A Gold Nanoparticle Based Colorimetric and Fluorescent Dual-Channel Probe for Acetylcholinesterase Detection and Inhibitor Screening. *RSC Adv.* **2018**, *8*, 32893-32898.
- 37. Flatebo, C.; Collins, S. S. E.; Hoener, B. S.; Cai, Y. Y.; Link, S.; Landes, C. F. Electrodissolution Inhibition of Gold Nanorods with Oxoanions. *J. Phys. Chem. C* **2019**, *123*, 13983-13992.
- 38. Zheng, T. Y.; Bott, S.; Huo, Q. Techniques for Accurate Sizing of Gold Nanoparticles Using Dynamic Light Scattering with Particular Application to Chemical and Biological Sensing Based on Aggregate Formation. *ACS Appl. Mater. Interfaces* **2016**, *8*, 21585-21594.
- 39. Li, T.; Senesi, A. J.; Lee, B. Small Angle X-ray Scattering for Nanoparticle Research. *Chem. Rev.* **2016**, *116*, 11128-11180.
- 40. Boles, M. A.; Engel, M.; Talapin, D. V. Self-Assembly of Colloidal Nanocrystals: From Intricate Structures to Functional Materials. *Chem. Rev.* **2016**, *116*, 11220-11289.
- 41. Baker, J. L.; Jimison, L. H.; Mannsfeld, S.; Volkman, S.; Yin, S.; Subramanian, V.; Salleo, A.; Alivisatos, A. P.; Toney, M. F. Quantification of Thin Film Crystallographic Orientation Using X-ray Diffraction with an Area Detector. *Langmuir* **2010**, *26*, 9146-9151.
- 42. Grulke, E. A.; Yamamoto, K.; Kumagai, K.; Hausler, I.; Osterle, W.; Ortel, E.; Hodoroaba, V. D.; Brown, S. C.; Chan, C.; Zheng, J., et al. Size and Shape Distributions of Primary Crystallites in Titania Aggregates. *Adv. Powder Technol.* **2017**, *28*, 1647-1659.
- 43. Xuan, Y. M.; Li, Q.; Hu, W. F. Aggregation Structure and Thermal Conductivity of Nanofluids. *AlChE J.* **2003**, *49*, 1038-1043.
- 44. Witten, T. A.; Sander, L. M. Diffusion-Limited Aggregation, a Kinetic Critical Phenomenon. *Phys. Rev. Lett.* **1981**, *47*, 1400-1403.
- 45. Fry, D.; Chakrabarti, A.; Kim, W.; Sorensen, C. M. Structural Crossover in Dense Irreversibly Aggregating Particulate Systems. *Phys. Rev. E: Stat., Nonlinear, Soft Matter Phys.* **2004**, *69*, 061401.
- 46. Oh, C.; Sorensen, C. M. Structure Factor of Diffusion-Limited Aggregation Clusters: Local Structure and Non-Self-Similarity. *Phys. Rev. E* **1998**, *57*, 784-790.

- 47. Lattuada, M.; Wu, H.; Sandkuhler, P.; Sefcik, J.; Morbidelli, M. Modelling of Aggregation Kinetics of Colloidal Systems and its Validation by Light Scattering Measurements. *Chem. Eng. Sci.* **2004**, *59*, 1783-1798.
- 48. Laramy, C. R.; Brown, K. A.; O'Brien, M. N.; Mirkin, C. A. High-Throughput, Algorithmic Determination of Nanoparticle Structure from Electron Microscopy Images. *ACS Nano* **2015**, *9*, 12488-12495.
- 49. Pyrz, W. D.; Buttrey, D. J. Particle Size Determination Using TEM: A Discussion of Image Acquisition and Analysis for the Novice Microscopist. *Langmuir* **2008**, *24*, 11350-11360.
- 50. Woehrle, G. H.; Hutchison, J. E.; Ozkar, S.; Finke, R. G. Analysis of Nanoparticle Transmission Electron Microscopy Data using a Public-Domain Image-Processing Program, Image. *Turk. J. Chem.* **2006**, *30*, 1-13.
- 51. Anane-Fenin, K.; Akinlabi, E. T.; Perry, N. Quantification of Nanoparticle Dispersion Within Polymer Matrix using Gap Statistics. *Mater. Res. Express* **2019**, *6*, 075310.
- 52. Tebbe, M.; Mayer, M.; Glatz, B. A.; Hanske, C.; Probst, P. T.; Muller, M. B.; Karg, M.; Chanana, M.; Konig, T. A.; Kuttner, C., et al. Optically Anisotropic Substrates via Wrinkle-Assisted Convective Assembly of Gold Nanorods on Macroscopic Areas. *Faraday Discuss.* **2015**, *181*, 243-260.
- 53. Goldstein, J. I.; Newbury, D. E.; Echlin, P.; Joy, D. C.; Lyman, C. E.; Lifshin, E.; Sawyer, L.; Michael, J. R. *Scanning Electron Microscopy and X-Ray Microanalysis*; 3rd ed.; Springer US: Boston, MA, 2003.
- 54. Sezgin, M.; Sankur, B. Survey Over Image Thresholding Techniques and Quantitative Performance Evaluation. *J. Electron. Imaging* **2004**, *13*, 146-168.
- 55. Otsu, N. A Threshold Selection Method from Gray-Level Histograms. *IEEE Trans. Syst. Man Cybern.* **1979**, *9*, 62-66.
- 56. Malpica, N.; de Solorzano, C. O.; Vaquero, J. J.; Santos, A.; Vallcorba, I.; Garcia-Sagredo, J. M.; del Pozo, F. Applying Watershed Algorithms to the Segmentation of Clustered Nuclei. *Cytometry* **1997**, *28*, 289-297.
- 57. Beucher, S. The Watershed Transformation Applied to Image Segmentation. *Scanning Microsc.* 6 1992.
- 58. Soille, P. *Morphological Image Analysis: Principles and Applications*; 2nd ed.; Springer Berlin Heidelberg: 2004.
- 59. Zafari, S.; Eerola, T.; Sampo, J.; Kälviäinen, H.; Haario, H. Segmentation of Partially Overlapping Nanoparticles Using Concave Points. In *Advances in Visual Computing*, Springer International Publishing: 2015; pp 187-197.
- 60. Park, C.; Huang, J. Z.; Ji, J. X.; Ding, Y. Segmentation, Inference and Classification of Partially Overlapping Nanoparticles. *IEEE Trans. Pattern Anal. Mach. Intell.* **2013**, *35*, 669-681.
- 61. Arganda-Carreras, I.; Kaynig, V.; Rueden, C.; Eliceiri, K. W.; Schindelin, J.; Cardona, A.; Sebastian Seung, H. Trainable Weka Segmentation: a Machine Learning Tool for Microscopy Pixel Classification. *Bioinformatics* **2017**, *33*, 2424-2426.
- 62. Lanzon, M.; Garcia-Vera, V. E.; Tenza-Abril, A. J.; De Stefano, V. Use of Image Analysis to Evaluate Surface Dispersion and Covering Performance of Nanolime Coatings Sprayed on Heritage Material Substrates. *Appl. Surf. Sci.* **2019**, *480*, 962-968.
- 63. Abdelsamea, M. M.; Pitiot, A.; Grineviciute, R. B.; Besusparis, J.; Laurinavicius, A.; Ilyas, M. A Cascade-Learning Approach for Automated Segmentation of Tumour Epithelium in Colorectal Cancer. *Expert Syst. Appl.* **2019**, *118*, 539-552.

- 64. Wang, Q.; Gao, J.; Yuan, Y. A Joint Convolutional Neural Networks and Context Transfer for Street Scenes Labeling. *IEEE Trans. Intell. Syst. Technol. Syst.* **2018**, *19*, 1457-1470.
- 65. Underwood, S. J.; Gorham, J. M. *Challenges and Approaches for Particle Size Analysis on Micrographs of Nanoparticles Loaded onto Textile Surfaces*; National Institute of Standards and Technology: 2017; p 22.
- 66. Kaushik, V.; Lahiri, T.; Singha, S.; Dasgupta, A. K.; Mishra, H.; Kumar, U.; Kumar, R. Exploring Geometric Properties of Gold Nanoparticles Using TEM Images to Explain Their Chaperone Like Activity for Citrate Synthase. *Bioinformation* **2011**, *7*, 320-323.
- 67. Meng, D.; Kumar, S. K.; Cheng, S. F.; Grest, G. S. Simulating the Miscibility of Nanoparticles and Polymer Melts. *Soft Matter* **2013**, *9*, 5417-5427.
- 68. Liu, K.; Nie, Z.; Zhao, N.; Li, W.; Rubinstein, M.; Kumacheva, E. Step-Growth Polymerization of Inorganic Nanoparticles. *Science* **2010**, *329*, 197-200.
- 69. Chen, Q.; Cho, H.; Manthiram, K.; Yoshida, M.; Ye, X. C.; Alivisatos, A. P. Interaction Potentials of Anisotropic Nanocrystals from the Trajectory Sampling of Particle Motion using in Situ Liquid Phase Transmission Electron Microscopy. *ACS Cent. Sci.* **2015**, *1*, 33-39.
- 70. Jain, P. K.; Eustis, S.; El-Sayed, M. A. Plasmon Coupling in Nanorod Assemblies: Optical Absorption, Discrete Dipole Approximation Simulation, and Exciton-Coupling Model. *J. Phys. Chem. B* **2006**, *110*, 18243-18253.
- 71. Abtahi, S. M.; Burrows, N. D.; Idesis, F. A.; Murphy, C. J.; Saleh, N. B.; Vikesland, P. J. Sulfate-Mediated End-to-End Assembly of Gold Nanorods. *Langmuir* **2017**, *33*, 1486-1495.
- 72. Wang, D.; Hore, M. J.; Ye, X.; Zheng, C.; Murray, C. B.; Composto, R. J. Gold Nanorod Length Controls Dispersion, Local Ordering, and Optical Absorption in Polymer Nanocomposite Films. *Soft Matter* **2014**, *10*, 3404-3413.
- 73. Thompson, C. V. Solid-State Dewetting of Thin Films. *Annu. Rev. Mater. Res.* **2012**, *42*, 399-434.
- 74. Smith, K. W.; McCarthy, L. A.; Alabastri, A.; Bursi, L.; Chang, W. S.; Nordlander, P.; Link, S. Exploiting Evanescent Field Polarization for Giant Chiroptical Modulation from Achiral Gold Half-Rings. *ACS Nano* **2018**, *12*, 11657-11663.
- 75. Deng, G. A Generalized Unsharp Masking Algorithm. *IEEE Trans. Image Process.* **2011**, 20, 1249-1261.
- 76. Yang, X. D.; Li, H. Q.; Zhou, X. B. Nuclei Segmentation Using Marker-Controlled Watershed, Tracking Using Mean-Shift, and Kalman Filter in Time-Lapse Microscopy. *IEEE Trans. Circuits Syst. I Reg. Papers* **2006**, *53*, 2405-2414.
- 77. Juve, V.; Cardinal, M. F.; Lombardi, A.; Crut, A.; Maioli, P.; Perez-Juste, J.; Liz-Marzan, L. M.; Del Fatti, N.; Vallee, F. Size-Dependent Surface Plasmon Resonance Broadening in Nonspherical Nanoparticles: Single Gold Nanorods. *Nano Lett.* **2013**, *13*, 2234-2240.
- 78. Mondini, S.; Ferretti, A. M.; Puglisi, A.; Ponti, A. Pebbles and PebbleJuggler: Software for Accurate, Unbiased, and Fast Measurement and Analysis of Nanoparticle Morphology from Transmission Electron Microscopy (TEM) Micrographs. *Nanoscale* **2012**, *4*, 5356-5372.

FOR TABLE OF CONTENTS ONLY

